# Understanding of strain-induced crystallization developments scenarios for polyesters: Comparison of poly(ethylene furanoate), PEF, and poly(ethylene terephthalate), PET

Emilie Parriaux Forestier, Christelle Combeaud, Nathanaël Guigo, Nicolas Sbirrazzuoli, Noëlle Billon

# Understanding of strain-induced crystallization developments scenarios for polyesters : comparison of poly(ethylene furanoate), PEF, and poly(ethylene terephthalate), PET

Emilie Forestier[a,b,c], Christelle Combeaud[a], Nathanael Guigo[b], Nicolas Sbirrazzuoli[b], Noelle Billon[a]

[a]MINES ParisTech, PSL Research University, CNRS, Centre de Mise en Forme des Matériaux (CEMEF), UMR 7635, 06904 Sophia Antipolis Cedex, France

[b] Université Côte d'Azur, CNRS, Institut de Chimie de Nice (ICN), UMR 7272, 06108 Nice Cedex 2, France

[c] Agence de l'environnement et de la Maîtrise de l'Energie 20, avenue du Grésillé- BP 90406 49004 Angers Cedex 01 France

*Corresponding author:

noelle.billon@mines-paristech.fr

**Keywords: biobased polymer, poly(ethylene 2,5-furandicarboxylate), poly(ethylene terephthalate), loading and unloading mechanical behaviour, viscoelasticity, strain induced crystallization, crystallization kinetics.**

## Abstract

Specific conditions of strain, stretching, strain rate and temperature are known to be necessary for the strain induced crystallization phenomenon (SIC) to occur. It leads to the formation of a crystal in different amorphous polymers, stretched above their glassy transition. This phenomenon was intensively documented in case of poly(ethylene terephthalate), PET. More recently, some studies focused on SIC development in biobased poly(ethylene furandicarboxylate), PEF. Comparison of these crystallization abilities and crystallization kinetics upon stretching in the two materials allows to describe main differences between them, and to enlighten the role of chain architecture on SIC. To achieve that point, different mechanical tensile tests were conducted using well controlled loading paths to explore the different steps of the microstructural changes induced by the stretching and their correlation with mechanical behaviour.

Several macroscopic equivalence in the effects of SIC were found, such as increase in modulus, appearance of organised phase, increase I n $\alpha$–relaxation temperature despite some

differences in chain architecture. Combining both loading-unloading tests and quenching protocols, it was found that inducing more or less strong interactions between constitutive units, and more or less stable crystalline phases, leads to differences in apparent strain induced crystallization kinetics:

- PET stretching can induce, prior to main strain hardening step, the formation of re-enforcing intermediate phases (or imperfect crystal) being stable upon unloading and able to be improved upon relaxation or thermal treatments;
- PEF stretching exhibits a more "simple" two-steps path with no intermediate phases stable upon unloading.

This can be related with the weaker stability of PEF crystal compared to PET (PEF quiescent crystallisation temperature and melting temperature are very close to each other), and to the more complex crystalline lattice in PEF (two units are needed instead of one due to furanic cycle). In addition, for PET, Young modulus increases more gradually during strain hardening than for PEF. The final microstructure after stretching is therefore more dependent on thermomechanical treatments (annealing or relaxation steps) in PET in comparison to PEF.

## 1. Introduction

The microstructure of polymers such as poly(ethylene terephthalate), named PET, or poly(ethylene furandicarboxylate), named PEF, can be modified when they are intensively stretched from their amorphous state and above their $\alpha$ relaxation temperature [1–9].

This temperature is around 80 °C and around 90 °C for PET and PEF, respectively. When polymers are uniaxially stretched, entangled chains are extended along one direction which can promote the nucleation of an anisotropic crystalline microstructure: this phenomenon is known as the strain induced crystallization (SIC). Formation of a crystalline structure is responsible for an improvement of the mechanical, thermal and barrier properties of the material. This ability to be stretched up to high strain (e.g., 120 %) and to crystallize under mechanical loading ("stretch ability" in the following) for polymers such as PET and PEF, is of prime interest in industry and especially for bottle forming with injection stretch blow moulding process (ISBM).

The present study aims at addressing that stretch ability for PEF, in comparison to that of PET, with the ultimate goal of accompanying future optimization of the use of PEF for bottle blowing in classical ISBM. To achieve that point, well controlled mechanical tests have to be performed in a relevant range of temperature and strain rate. Then, microstructure evolution has to be explored.

Additionally, as far as loading path is concerned, ISBM is a complex process in which uniaxial and biaxial loadings co-exist. Uniaxial tension even precedes biaxial loading due to the pre-blow stretching. So, it would be tempting to address both some uni and bi axial (sequential and simultaneous) loadings in our study. However, controlling local mechanical conditions (strain rate and uniformity of strain or stress) as well as measurement of local stress during biaxial tests are still difficult, especially above Tg.

In consequence, as on one hand uniaxial tension is part of the ISBM process and, on the other hand and more importantly, is still the best first step for studying stretch ability of polymers, we will focus on simple tension in this paper.

Within this frame, the first step is the knowledge of the strain rate and the temperature conditions for which SIC occurs as this latter controls maximum draw ratio that can be reached as well as final properties of the bottle. PET, which is the most widely used polymer in ISBM, was reported to exhibit different stable or metastable phases, named "mesophases" (or crystal precursor of various perfection or completion), along stretching path [10–14]. The different conformational changes that are necessary, either to extend the chains or to promote crystallization, have been depicted combining different techniques (X-ray diffraction, IR, RAMAN or UV spectrometry) (see [4] for a rapid overview).

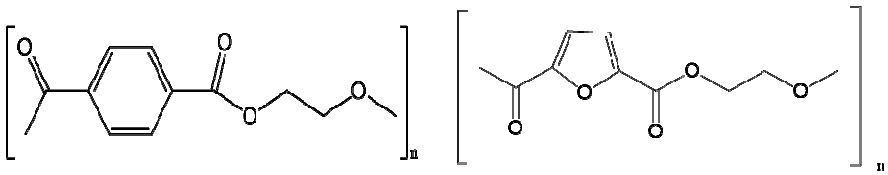

Figure 1: Molecular structures of PET (left) and PEF (right)

Roughly, upon stretching for PET, $C_6$ ring can easily be flipped to be coplanar to the loading plane. Then, the *gauche* conformation around the ester group can be changed to the *trans* conformation, which is the only one remaining in crystalline zones. This contribute to promote or accelerate the cold crystallization (i.e., crystallization from solid quenched amorphous state), which is SIC.

PEF is considered as the biobased counterpart of PET, but its relative novelty does not allow same level of certainness. Indeed, from a microstructural point of view, the main difference between PEF and PET is the presence of the furan cycle, whose flip is not easily authorized, contrary to the benzenic ring present in PET (Figure 1). Consequently, in the case of PEF, this difference does constrain conformational changes necessary for crystallization.

These differences in molecular structures result in a higher stiffness, a lower crystallization rate and better barrier properties for PEF compared to PET [15–21]. Up to now, no studies were reported on the crystal development of PEF under uniaxial stretching.

PET crystal structure was described by Daubeny et al. as a triclinic system [22]. PEF crystal unit cell was firstly proposed as a triclinic one [23] and was recently defined as a monoclinic one by Mao et al. [3]. A crystallographic analysis of uniaxially stretched PEF was depicted in previous work [24], in which the crystalline structure of stretched PEF was compared to that obtained after quiescent crystallization. The same crystalline organization was found. This could mean that PEF exhibits a unique crystalline phase contrary to proposal of Stoclet et al. [1] who reported a possible mesophase. This contradiction must be deepened. Anyway, all the crystalline families were indexed according to the monoclinic cell proposed by Mao et al [3].

Araujo et al. [25] analysed the conformational changes observable during PEF quiescent crystallization as well as crystallization induced by a solvent. In addition to the change of ethylene glycol from *gauche* to *trans* conformations (as in PET), the furan ring in PEF introduces a possible change from *anti* to *syn* conformations. A recently submitted paper, [26] compared the conformations present in stretched PEF and PET to those obtained during quiescent crystallizations. It was demonstrated that strain induced crystallization does lead to more constrained group compared to static crystallization, which was explained by chain extension and packing effect.

Even though some synchrotron analysis exists in the literature [1–3], microstructural development and its kinetic in PEF under stretching has not yet been totally investigated.

This present paper aims at a deeper description and comparison of the microstructural evolutions involved during uniaxial tensions performed in equivalent conditions for PET and PEF. Uniaxial tensile tests were chosen as a first approach to enforce changes in microstructure. Based on previous results on PET [4], samples were stretched, at given temperature and strain-rate, up to a controlled strain and quenched either immediately after the end of the stretching, or after an additional controlled unloading step. Samples quenched before unloading are referred as “interrupted” in the following, while samples quenched after unloading are referred as “unloaded”. Quenching was performed with cold air, which was enough to impose a cooling rate of - 1000 °C/min. The shape of the unloading loop gives information on the amount of remaining degree of viscoelasticity after stretching. This degree of viscoelasticity is assumed to decrease with the progression of crystallization. Finally, the microstructure in the different samples, i.e. “interrupted” and “unloaded”, were analysed to suggest a possible schematic of structure development under stretching. The comparison

between the two kinds of post stretching treatment, “interrupted” and “unloaded”, allows estimating the potential microstructural evolution taking place during the unloading path.

## 2. Materials and Methods

### 2.1 Materials

Poly(ethylene 2,5-furandicarboxylate) was synthetized from the direct esterification and melt-solid state polycondensation (SSP) of monoethylene glycol and 2,5-furandicarboxylic acid (FDCA) produced by Avantium Renewable Polymers. Extruded PEF sheets with a thickness of 700 µm have been provided. Samples were extracted in the extrusion direction, to minimize thickness variation.

A commercially available PET grade (RamaPET N180® from Indorama) supplied by Sidel company was extruded into PET sheets by Avantium Renewable Polymers with a thickness of 700 µm. Samples were extracted in the extrusion direction too.

Extrusions were performed according to state of the art after drying to avoid hydrolysis and degradation.

Samples were stored under vacuum in an aluminium coated bag, in the freezer (-18 °C), to avoid water absorption and physical aging. Consequently, materials were tested dry, as processed, without any pre-conditioning.

### 2.2 Mechanical tests

A homemade device designed for film stretching under controlled temperature conditions was used. It can reproduce industrial uniaxial and biaxial stretching conditions. It is composed of four independent motor-driven arms, each coupled to a displacement sensor and a 500 N force transducer. Tensile velocity was ruled to keep strain rate, $\dot{\varepsilon}_0$, as constant as possible in the central zone of the samples. To this purpose, velocity varied exponentially with time and same strain rate was used during loading and unloading paths.

The sample can be heated and, annealed or quenched after stretching, with several mobile ovens. A window of zinc selenide (ZnSe), which is partially transparent to infrared radiations, allows to measure the temperature at the surface of the specimen during tests. On the other face of the sample, another borosilicate glass window allows local measurements of strain fields using DIC (2D Digital Image Correlation) on painted speckle. It was shown that adding a painted speckle of thickness of almost 40 µm did not impact force measurement. DIC was used to address local Hencky’s strain, on the specimen surface and in the two directions (transversal and longitudinal). Mechanical tests were analysed in terms of true stress

(calculated using the actual instantaneous section), and true strain as depicted by Equation 1. Transverse isotropy hypothesis was assumed.

$$\sigma(t) = \frac{F(t)}{e_0 * w_0 * exp(2\varepsilon_{yy}(t))} \quad (1)$$

with, $w_0$ and $e_0$ the initial width and thickness and $\varepsilon_{yy}(t)$ and F(t) the lateral strain, i.e. in the direction perpendicular to the tensile direction and the force at time t, respectively.

For each measurement, an IR pyrometer and a CCD camera were synchronised to the other analogic signals (force, displacement…). In any case, material was quenched after tests to freeze the microstructure. The paint was then mechanically removed for post-stretching analysis, that were performed at the same location as mechanical analysis on the sample, i.e. the central zone where local stress and strain were measured.

## 2.3 Stretching conditions determination

To fit with the industrial process, stretching has to be performed above the $\alpha$-relaxation temperature and below the onset temperature of the cold crystallization. These temperatures were estimated by Dynamic Mechanical Thermal Analysis (DMTA) for the two polymers.

All DMTA experiments were conducted in tension using a Mettler-Toledo® DMA 1. The dimensions of the samples were 5 x 4 x 0.7 $mm^3$ for amorphous samples and around 5 x 3 x 0.3 $mm^3$ for stretched samples (depending on the total strain imposed). At the beginning of each test, the sample underwent a preload of 1 N. Temperature scans were performed between 25 °C and 200 °C, at a heating rate of 1 °C/min, with a displacement amplitude of 5 µm (i.e. strain of 0.1 %), in auto-tension mode. Linearity of the behaviour was checked prior to all tests. Temperature scans were carried out at a frequency of 1 Hz. The $\alpha$-relaxation temperature, taken at the maximum of tan(δ) peak, were respectively of 80 °C for PET and of 92 °C for PEF, while cold crystallization was detected for a temperature close to 110 °C for PET and to 160 °C for PEF (Figure 2).

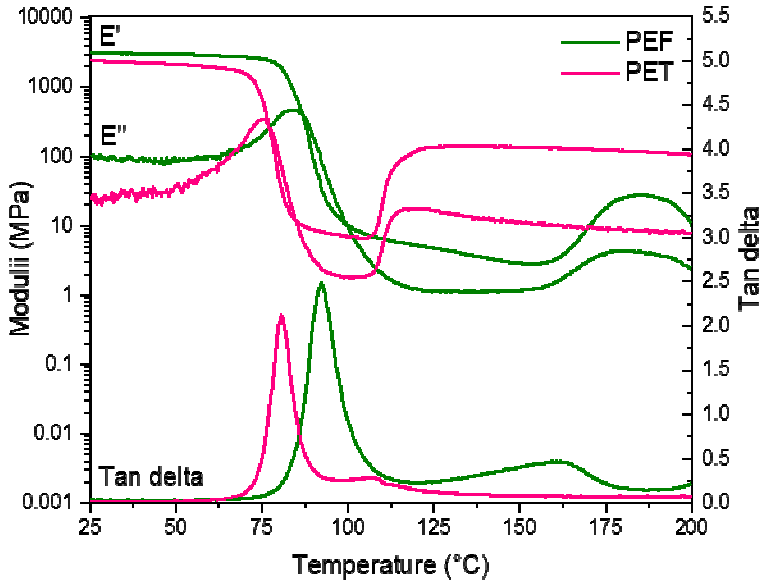


Figure 2. DMTA temperature scans of amorphous PEF (in green) and PET (in pink), for a heating rate of 1°C/min and a frequency of 1Hz, in a tensile mode.

Moduli in the rubbery state are close for the two polymers though PET exhibits a slightly higher modulus [27], which can be explained by a higher density of entanglements [27,28]. To define stretching temperatures and strain rates, differences in α-relaxation temperature had to be accounted for. As we aimed at comparing the two polymers in identical physical state, decision was made not to stretch polymers at the same temperature and strain rate but at a similar equivalent strain rate at a reference temperature chosen close to their respective glass transition temperature.

As a result, the same method as validated in previous studies [24,29], was used: frequency scans were conducted at various temperatures to build up master curves at two different reference temperatures of 100 °C and 90 °C for PEF and PET, respectively (Figure 3.a).

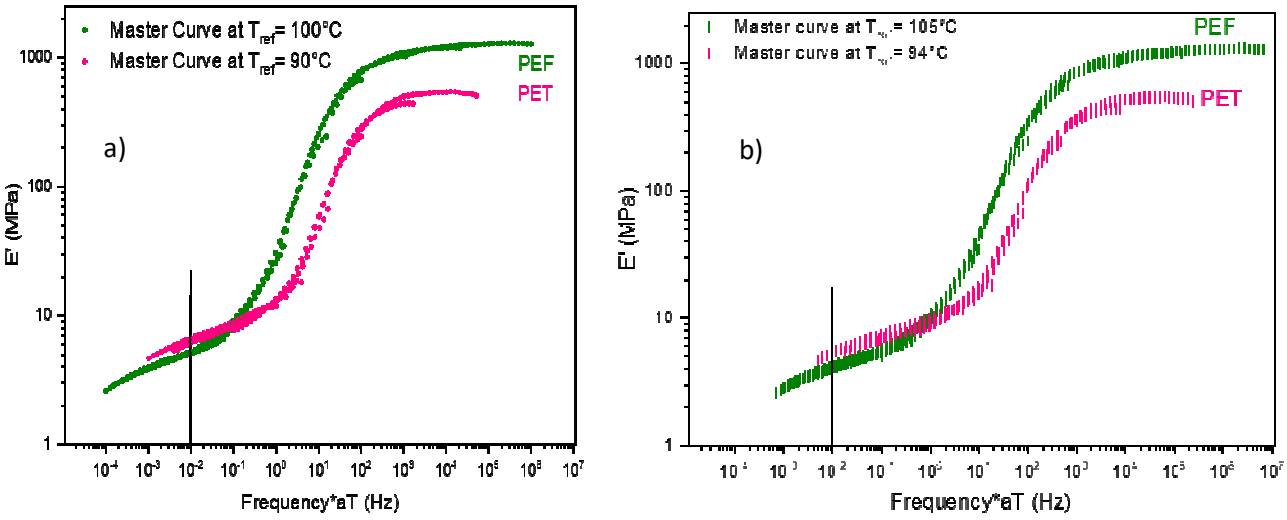


Figure 3. Master curves of amorphous PEF and PET at different reference temperatures: (a) reference temperatures close to $T_g$ (reference of 100°C for PEF and 90 °C for PET); (b) reference temperatures close to testing temperature (105°C for PEF and 94 °C for PET).

An equivalent strain rate close to $T_g$ of 0.01 $s^{-1}$ was chosen, whose order of magnitude corresponds to processing range. For convenience, technological conditions of strain rate and temperature were chosen as follows: (0.07 $s^{-1}$ at 105°C) for PEF and (0.05 $s^{-1}$ at 94°C) for PET. These conditions correspond to the middle of the PEF processing range and to the terminal part of the rubbery plateau for PET (before the flowing region) as confirmed by master curves at testing temperatures as reference (Figure 3.b).

## 2.4 Loading and unloading conditions

Figure 4.a depicts typical stress-strain curves of PEF and PET. Both materials exhibit the same type of behaviour, with a drastic strain hardening at true strains of 1.56 for PET and 1.82 for PEF. This defines a natural draw ratio (NDR) of 4.76 and 6.17 for PET and PEF, respectively. PEF exhibits a strain hardening with a higher slope and a higher level of stress than PET [26].

Materials were stretched up to different representative local strains in the centre of the sample:

1- Far from NDR ($\varepsilon_{xx} = 0.90$ for PET and $\varepsilon_{xx} = 1.20$ for PEF);
2- Close but before NDR ($\varepsilon_{xx} = 1.45$ for PET and $\varepsilon_{xx} = 1.75$ for PEF);
3- Close but after NDR ($\varepsilon_{xx} = 1.60$ for PET and $\varepsilon_{xx} = 1.93$ for PEF);
4- Far from NDR ($\varepsilon_{xx} = 1.72$ for PET and $\varepsilon_{xx} = 2.06$ for PEF);
5- After rupture ($\varepsilon_{xx} = 1.94$ for PET and $\varepsilon_{xx} = 2.12$ for PEF)

These different conditions are marked on the mechanical curves in Figure 4.b and 4.c for PET and PEF, respectively.

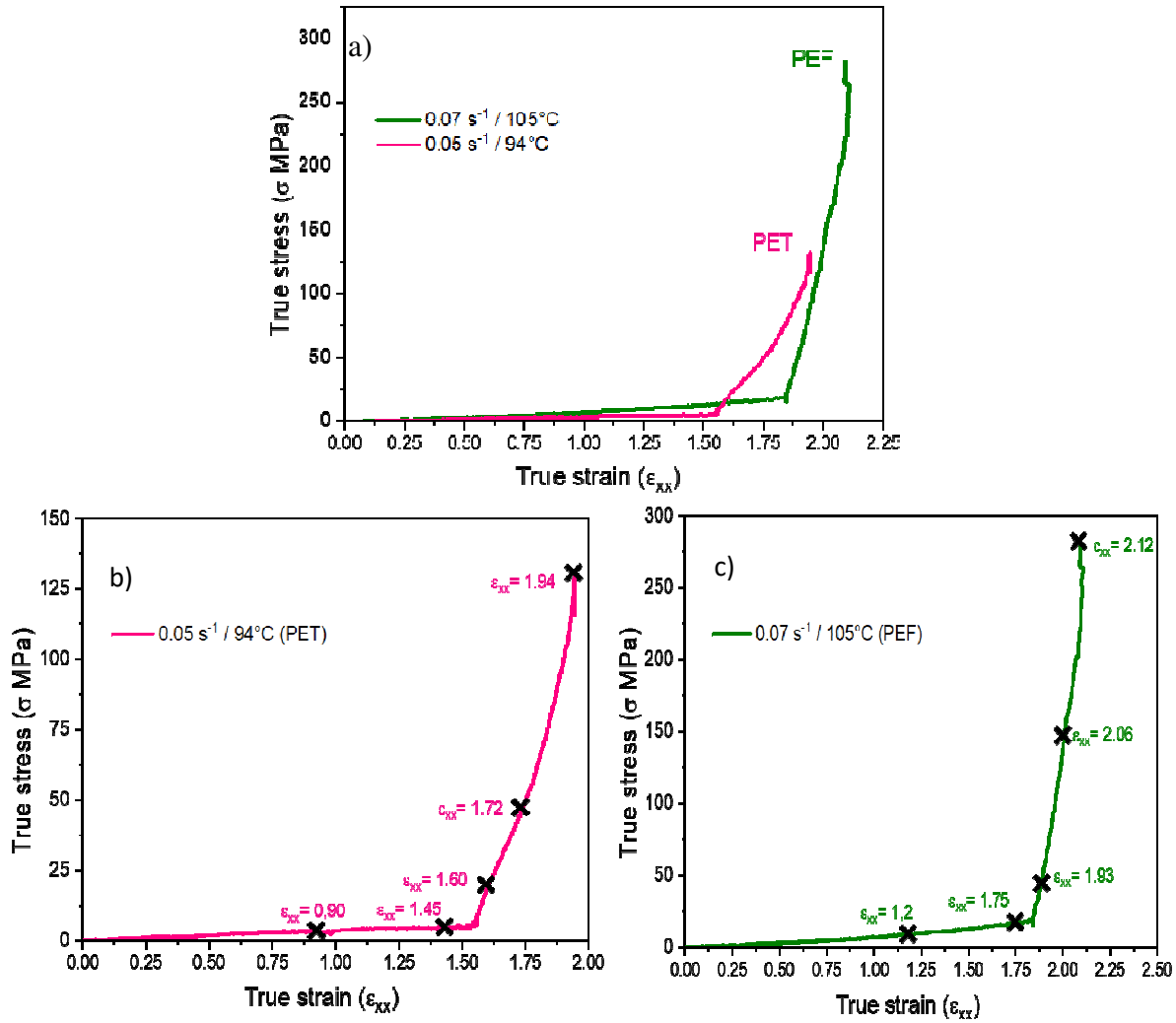


Figure 4. (a) True stress/strain curves of PEF and PEF under uniaxial stretching; description of the mechanical conditions for (b) PET and (c) PEF

Table 1 summarizes conditions that were explored for the "interrupted" and the "unloaded" tests and for both PET and PEF. Grey boxes correspond to the non-explored cases (i.e only interrupted or only unloaded). For "interrupted" tests, specimens were firstly air-quenched to room temperature just after stretching and, secondly, unloaded. In case of "unloaded samples" unloading step was performed at same strain rate as loading step down to a zero force at the temperature of the test and, then, air quenched without any additional delay. Main objective was to release the stress while avoiding buckling or compression that would have damaged the sample. A consequence of this is that the unloading time depends on the amount of an-elasticity developed during loading compared to final strain. Looking at unloading steps in

Figures 5 and 6, one can estimate unloading time as the final strain reached minus the residual strain at zero force divided by the strain rate. Finally, unloading time ranged from 13 s to less than 0.1 s depending on samples, being the unloading time longer in case of stretching below NDR (Table 1) and close to 0 in case of stretching above NDR. In summary, this uncertainness could have led to an overestimate of crystallization in sample 1 of above list, which did not reveal significant crystallization, and is neglectable in case of samples 2 to 4.

| **PET** | | | | | |
|---|---|---|---|---|---|
| Unloaded | $\varepsilon_{xx} = 0.90$ | $\varepsilon_{xx} = 1.45$ | $\varepsilon_{xx} = 1.60$ | $\varepsilon_{xx} = 1.72$ | |
| Unloading time (s) | 8 | 4 | <0.1 | <0.1 | |
| Interrupted | $\varepsilon_{xx} = 0.90$ | $\varepsilon_{xx} = 1.45$ | $\varepsilon_{xx} = 1.60$ | | $\varepsilon_{xx} = 1.94$ |
| **PEF** | | | | | |
| Unloaded | $\varepsilon_{xx} = 1.20$ | $\varepsilon_{xx} = 1.75$ | $\varepsilon_{xx} = 1.93$ | $\varepsilon_{xx} = 2.06$ | |
| Unloading time (s) | 13 | <0.2 | <0.1 | <0.2 | |
| Interrupted | $\varepsilon_{xx} = 1.20$ | $\varepsilon_{xx} = 1.75$ | $\varepsilon_{xx} = 1.93$ | | $\varepsilon_{xx} = 2.12$ |

Table 1. Summary of the mechanical tests performed in PET and PEF.

As mentioned before, and for all stretching conditions presented, the resulting microstructure has been characterized.

## 2.5 FTIR analysis

The microstructure was analysed by Fourier transform infrared spectroscopy (FT-IR) between 4000 $cm^{-1}$ and 600 $cm^{-1}$ with a Bruker TENSOR 27® spectrophotometer in absorbance mode using a diamond crystal. 64 scans were accumulated with a resolution of 4 $cm^{-1}$.

## 2.6 X-ray scattering analysis

Wide-angles X-ray scattering (WAXS) using CuKα radiation ($\lambda$ = 1.54 Å) was performed under vacuum at room temperature. 2D Debye-Scherrer patterns using the flat-film camera technique were recorded as a first experiment to enlighten the presence of crystalline phase and its orientation. The sample to screen distance was generally of 75 mm. Some additional measurements on PEF were performed with a distance of 30 mm, to detect crystalline families at higher angular positions. Exposure time was set to 45 minutes. 1D scans I(2θ) were carried out in transmission mode (from 5° to 50°), using a diffractometer Philips X'Pert PRO® supplied by Panalytical. Scattered intensities were normalised by the sample thickness, which depends on stretching conditions imposed.

Two radial scan directions have been explored: in the transverse and in the machine directions so as to quantify (hk0) and (00l) diffractions, respectively. On the commonly referred "equatorial direction", (hk0) families are observable, whereas on the "meridional direction" it is the (00l) crystalline families.

### 2.7 Thermal analysis

The crystallinity ratio ($\chi_{SIC}$) was evaluated by DSC, at a heating rate of 10K/min, performed on a Mettler-Toledo® 1, and calculated as defined in Equation 2:

$$\chi_{SIC} = \frac{\Delta Hm - |\Delta Hc|}{\Delta H_m^0} \qquad (2)$$

with $\Delta H_m$ the melting enthalpy, $\Delta H_c$ the cold crystallization enthalpy and $\Delta H_m^0$ the equilibrium melting enthalpy, taken at 140 $J.g^{-1}$ for PEF and PET [27,29,30].
Sample weight was about 3 mg and measurements were performed in aluminium pans.

## 3. Results and discussion

### 3.1 Mechanical behaviour and crystallization

Figures 5 and 6 respectively depict mechanical behaviour of PET and PEF for "unloaded" tests. For clarity, true stress/strain issuing from "interrupted" tests are not presented, as loading responses are pretty well superimposed to the "interrupted" ones accounting for experimental scattering.
Nevertheless, one has to emphasize that this scattering induced some apparent lack in reproducibility of NDR. Typical order of magnitude of such scattering can be estimated in Figure 5 by comparing stress-strain curves up to strain of 1.60 and 1.72 for PET. Main effect was observed on NDR, which was not surprising, as local strain rate is not controlled per se and is impacted by strain hardening itself that constrain local deformation. As a consequence, exact strain rate could vary from one sample to another as soon as strain hardening occurred. Indeed, even if technological loading rate is controlled in the same manner, local strain rate can depend on small local fluctuation in size (thickness), or microstructure, or temperature.
However, the minor differences noticed remain reasonable and do not modify the analysis.
The corresponding Debye-Scherrer patterns are associated to each test.

Finally, as enlightened by the initial Debye-Scherrer analysis both unstretched PEF and PET exhibited the expected isotropic amorphous microstructure. Following describes evolution in a phenomenological manner.

### 3.1.1 Case of PET

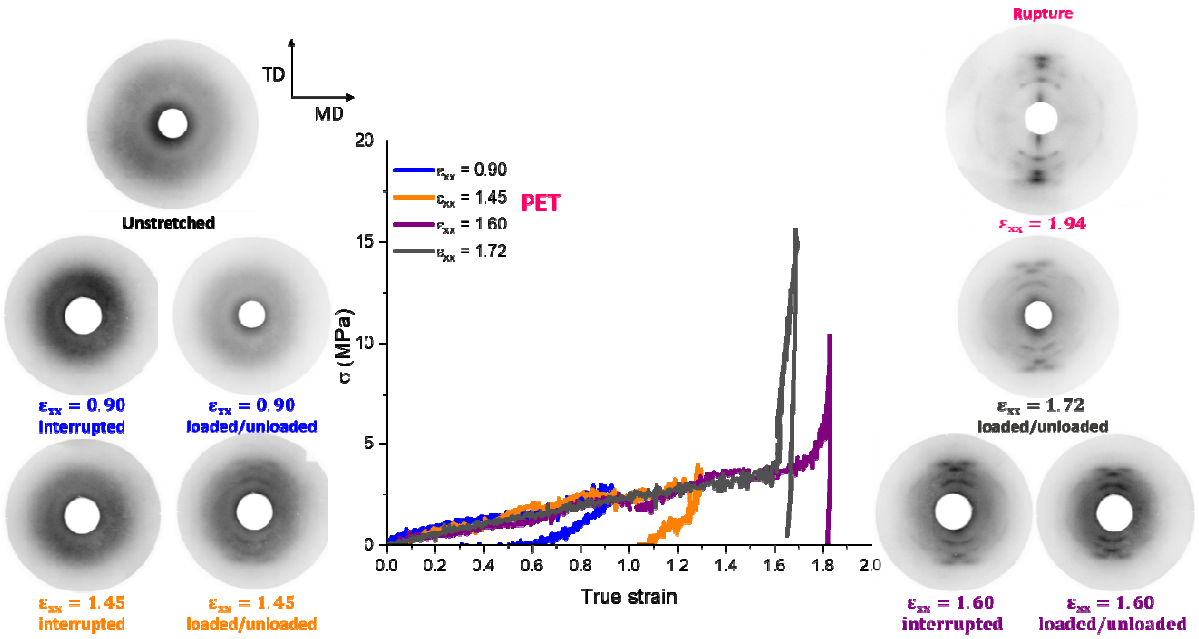


Figure 5. Loading/unloading true stress/strain curves of PET for strains up to 0.90; 1.45; 1.60 and 1.72. Comparison of Debye-Scherrer analysis before unloading ("interrupted" tests) and after unloading ("loaded/unloaded" and "rupture"). TD is the transverse direction while MD is machine (or stretching) direction.

Through the analysis of the two first unloading conditions ($\varepsilon_{xx}$ = 0.90 and $\varepsilon_{xx}$ = 1.45), PET exhibits a mainly visco-elastic behaviour, as previously observed [4,31,32]. There is some evidence for in-elasticity that could be confused with plasticity. However, material is not an elasto-viscoplastic body but mainly a visco hyperelastic polymer in this range. The existence of residual strain after unloading only suggests that some deformation was not recovered instantaneously after unloading. This does not prove the occurrence of plastic processes. In-elasticity can be related to visco elasticity (part of residual strain can be recovered within hours or days) and to first stage of SIC instead of plasticity. Concept of "blocked elastic energy" is more relevant. This latter can be related to entropic elasticity of chains locked by the precursors of crystallization as organization is very progressive in PET. An indirect proof is the comparison between unloading loop for PET (for which progressive organization is claimed in the paper) to that of PEF (for which a closer to a single crystallization process is

suggested) (Figures 5 and 6, respectively.). Unloading loops (for strain of 1.20) is almost closed for PEF, demonstrating a visco elastic behaviour.

The shape of the unloading is very different close to NDR. Then, the strain appears to be 100 % irreversible. Once again this is irreversible strain but not plasticity per se.

Debye-Scherrer patterns did not reveal well defined periodic organisation, i.e. crystallization, below strain of 1.60. However, whereas at low strain (0.90) diffraction pattern was a characteristic amorphous halo, there was some trace of periodicity (incomplete diffraction pattern) for strain of 1.45. This latter pattern was quite diffuse but organisation was clearly not isotropic and unloading at test temperature seemed to improve the microstructure (better definition of diffractions for unloaded samples). This will be completed in the paragraph "Crystalline development scenario" where more quantitative diffraction scans will be presented.

To conclude, at this level our observations suggest that tension induced some periodic arrangements (discrete nuclei or global organisation, this cannot be discriminated) in the material above strain of 1.45. Distribution is not isotropic and periodicity could be improved upon unloading without promoting a truly crystalline pattern. To go further, let's add that the first traces corresponding to (hk0) planes (in the equatorial direction), are seemingly oriented parallelly to the tensile axis. Some traces of even lower intensities of crystalline families close to the meridional direction, related to (00l) crystalline families, can be foreseen. This suggests that the chains were extended and oriented by tension and nucleated an organized phase (mesophase, crystal precursor or imperfect crystal) that develops toward crystal during unloading. This scenario has already been reported in the literature [4,33,34].

After NDR ($\varepsilon_{xx}$ = 1.60 and $\varepsilon_{xx}$ = 1.72), the mechanical response is different, the reversibility of deformation drastically decreases, suggesting a change in material microstructure. On Debye-Scherrer patterns, differences between strains of 1.45 and 1.6 are observed with an increase of spots intensity, which can be due to higher level of crystallinity. Once again, a more quantitative approach thanks to diffraction scans in the transverse direction does confirm this first analysis in the following paragraph "Crystalline development scenario". Indeed, when $\varepsilon_{xx}$ = 1.60, the formation of an anisotropic and periodic structure was observed, whatever the cooling conditions were. Once again, mainly equatorial (hk0) dots are visible. For the last unloading condition ($\varepsilon_{xx}$ = 1.72), an organized microstructure with intense spots in the equatorial direction is also present. The dots become more defined and less diffused after rupture. To understand that point one has to considered that rupture corresponds to unloading

of the sample. A better-defined crystal is then consistent with our observation concerning unloaded samples. This possible crystallization during unloading was already suggested in the past [4,32]. However, in that case quenching was not possible and, consequently cooling down after unloading is slower than in other tests which can favour crystallization too [4].

This can explain also that diffractions, such as ($\bar{1}11$), ($\bar{1}12$), ($\bar{1}03$) and ($0\bar{1}1$), different from (hk0) and (00l) ones, become observable.

For this case, it appears that the final microstructure is very close to the perfect fiber texture one, as referred in the literature by Liu & Geil [35,36].

To sum-up, our observations are coherent with the formation of the definitive crystal after the stretching in PET as reported in previous works [10–14], whereas strain hardening could be due to imperfect crystal, mesophase or precursors.

In any case, these observations confirm that the strain hardening, as well as the organized microstructure, appear step by step for PET.

### 3.1.2 Case of PEF

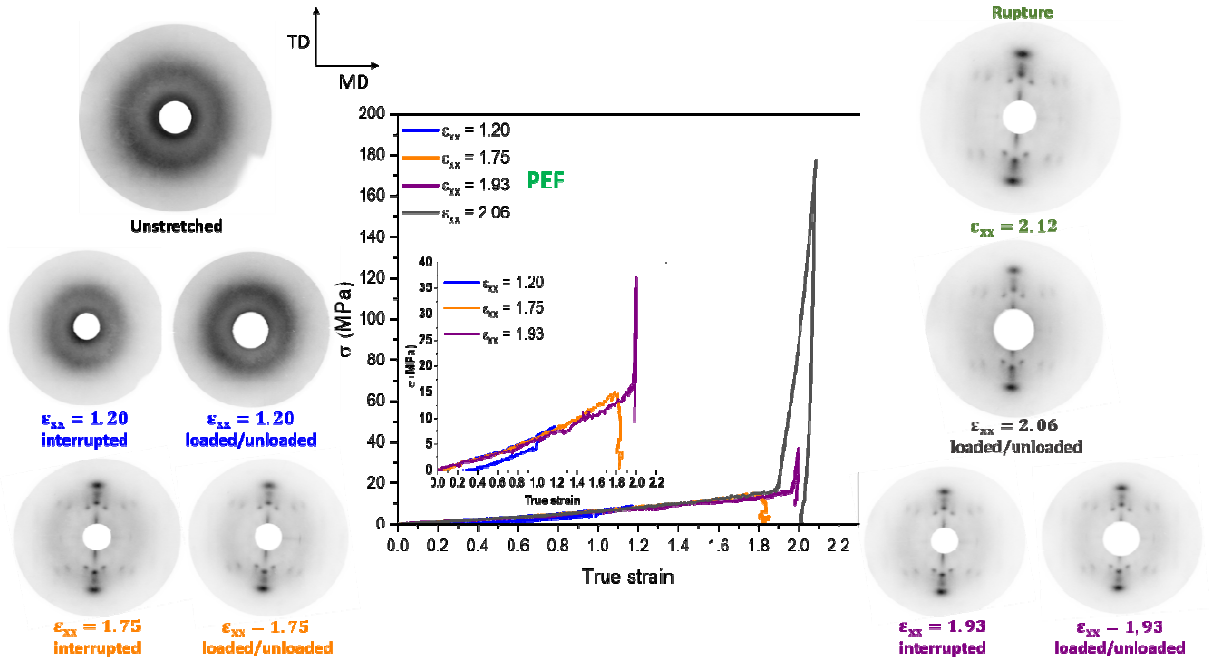


Figure 6. Loading/unloading true stress/strain curves of PEF for strains up to 1.20; 1.75; 1.93; and 2.06. Comparison of Debye-Scherrer analysis before unloading (“interrupted” tests) and after unloading (“loaded/unloaded” and “rupture”). TD is the transverse direction while MD is machine (or stretching) direction.

Stress developed in PEF reaches higher values than those reached in PET, even during the first deformation stage. Consequently, a zoom has been added for the first three unloading conditions ($\varepsilon_{x\,x}$= 1.20; $\varepsilon_{xx}$ = 1.75; $\varepsilon_{xx}$ = 1.93) in Figure 6.

The first unloaded test ($\varepsilon_{xx}$ = 1.20) leads to a visco-elastic loop, as discussed above, with a structure close to the amorphous state whatever the cooling conditions are (i.e. “interrupted” and “unloaded” tests). Closer to NDR (εxx = 1.75 and εxx = 1.93), the mechanical response seems “elasto-plastic”-like but same doubts as for PET concerning potential plastic processes exists. Whatever, at this stage, a well-defined crystalline structure is visible which is not sensitive to unloading conditions. This is obviously different from PET, as crystal structure already clearly defined appears at once prior to mechanical strain hardening (presence of intense and defined spots on Debye-Scherrer patterns). The fact that it was impossible to observe mesophase prior to crystallization is contradictory to previous assumptions [1]. Nevertheless, it is coherent with the sharper strain hardening slope and the higher NDR of PEF (Figure 4.b) compared to PET (Figure 4.a). It is also compatible with what can be imagine concerning crystallization of PEF. The predictable lower mobility of PEF chain and the symmetry of the furan ring (crystal is formed of segments composed by two repeating units [3] (instead of one) should contribute to make crystallization more difficult for PEF. The architecture of PEF chain should lead to weaker interactions between segments, that is, less stable crystal than PET one (suggested by the lower melting temperature too) but also less stable potential mesophases. One possible conclusion is then, that due to those characteristics, no intermediate organized metastable phases can be promoted in PEF that could contribute to harden the material. Strain hardening could occur only when conditions of complete crystallization are reached. On the contrary, PET can exhibit mesophase or early stage of crystallization whose life time is long enough to contribute to strain hardening. Then, strain hardening and development of its crystal can coexist. The “interrupted” and “unloaded” conditions at higher strain ($\varepsilon_{xx}$ = 1.93 and $\varepsilon_{xx}$ = 2.06) show that the microstructure seems accomplished, and is the same before and after the unload as well as after the rupture ($\varepsilon_{xx}$ = 2.12).

To conclude on this part, metastable phases of lower level of organization than final crystal exist in PET and contribute to strain hardening, making it more progressive. Whereas in PEF, final crystal has first to be stable, so that strain hardening can develop. As Debye-Scherrer only gives qualitative results, radial scans must be performed to further understand the crystalline development.

## 3.2 Crystalline development scenario

This part focuses on a possible scenario for SIC based on DSC and diffraction scans. DSC curves are depicted in Figure 7.a and 7.b, respectively and the resulting crystallinity ratios are gathered in Table 2. Diffraction scans are represented on Figures 8 to 10. Figures 8 to 10 show diffraction scans in the transverse direction (equatorial direction, analysis of (hk0) plans) for PET and PEF, respectively. The development of the $(\bar{1}05)$ diffraction in PET, associated to a plane perpendicular to chain axis, is represented in Figure 9 (machine direction or meridional direction). The results obtained scans agree previously reported data [31,32].

It was also reported for PEF [2,3,24] that, in uniaxial stretching conditions, many meridional diffractions are visible. These diffractions are diffuse with a low intensity. Accounting for the wave length used in this study, their angular positions are higher than 25°. They can be observed in our Debye-Scherrer device when the sample to screen distance is decreased down to 30 mm. These diffractions are visible in Figure 11.

| **PET** | | | | | |
|---|---|---|---|---|---|
| Interrupted | $\varepsilon_{xx} = 0.90$ | $\varepsilon_{xx} = 1.45$ | $\varepsilon_{xx} = 1.60$ | | $\varepsilon_{xx} = 1.94$ |
| $\chi$ (%) | 8 | 12 | 36 | | 47 |
| Unloaded | $\varepsilon_{xx} = 0.90$ | $\varepsilon_{xx} = 1.45$ | $\varepsilon_{xx} = 1.60$ | $\varepsilon_{xx} = 1.72$ | |
| $\chi$ (%) | 11 | 29 | 42 | 43 | |
| **PEF** | | | | | |
| Interrupted | $\varepsilon_{xx} = 1.20$ | $\varepsilon_{xx} = 1.75$ | $\varepsilon_{xx} = 1.93$ | | $\varepsilon_{xx} = 2.12$ |
| $\chi$ (%) | 0 | 27 | 28 | | 35 |
| Unloaded | $\varepsilon_{xx} = 1.20$ | $\varepsilon_{xx} = 1.75$ | $\varepsilon_{xx} = 1.93$ | $\varepsilon_{xx} = 2.06$ | |
| $\chi$ (%) | 0 | 32 | 35 | 34 | |

Table 2. Crystalline ratios evolution over stretching, for PEF and PET.

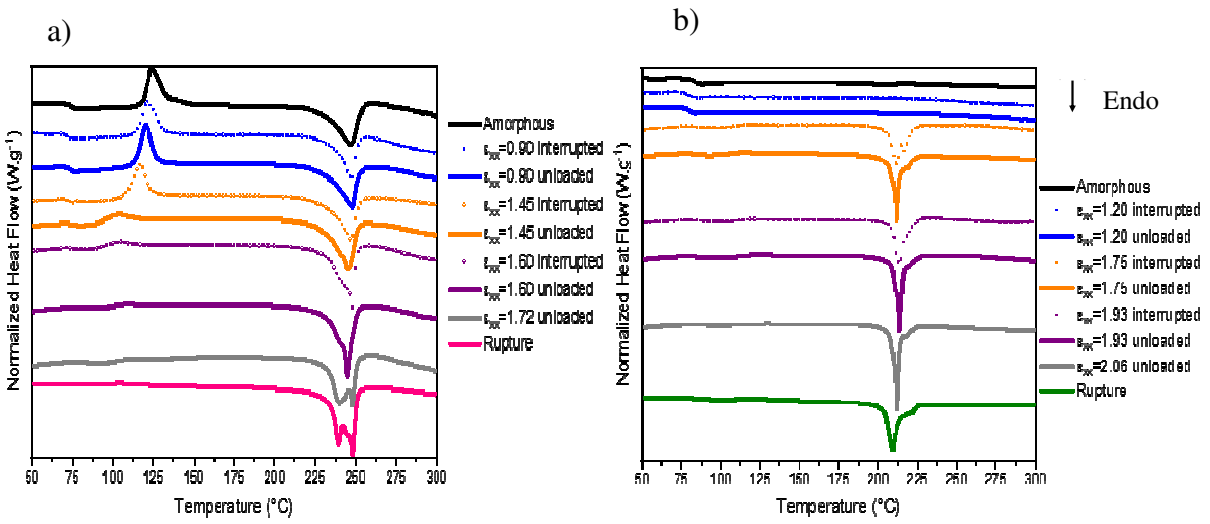


Figure 7. Typical DSC thermograms from 50°C to 300°C performed at a heating rate of 10°C/min for (a) PET and (b) PEF. Comparison between unloaded samples (plain lines) and interrupted samples (dotted lines). Endothermic phenomena are top-down.

Conclusions drawn from X-ray diffractions are confirmed through this analysis:

- SIC is a progressive phenomenon for PET as demonstrated by the progressive decrease of the enthalpy of cold crystallization with increasing strain;
- Pre-nucleation, due to the first stages of SIC in PET, is evidenced by a gradual decrease in cold crystallization temperature and a gradual increase of glass temperature;
- These evolutions are more marked when samples are unloaded before quenching;
- Melting peak, which is single peak-shaped when amorphous PET cold crystallizes progressively become double-peak shaped, suggesting two crystallization regimes (perhaps during loading and unloading).
- Schematic in PEF is much simpler being the material amorphous below NDR and crystalline above.

Next two following parts analyze the crystal formations thanks to radial scans.

### 3.2.1 PET

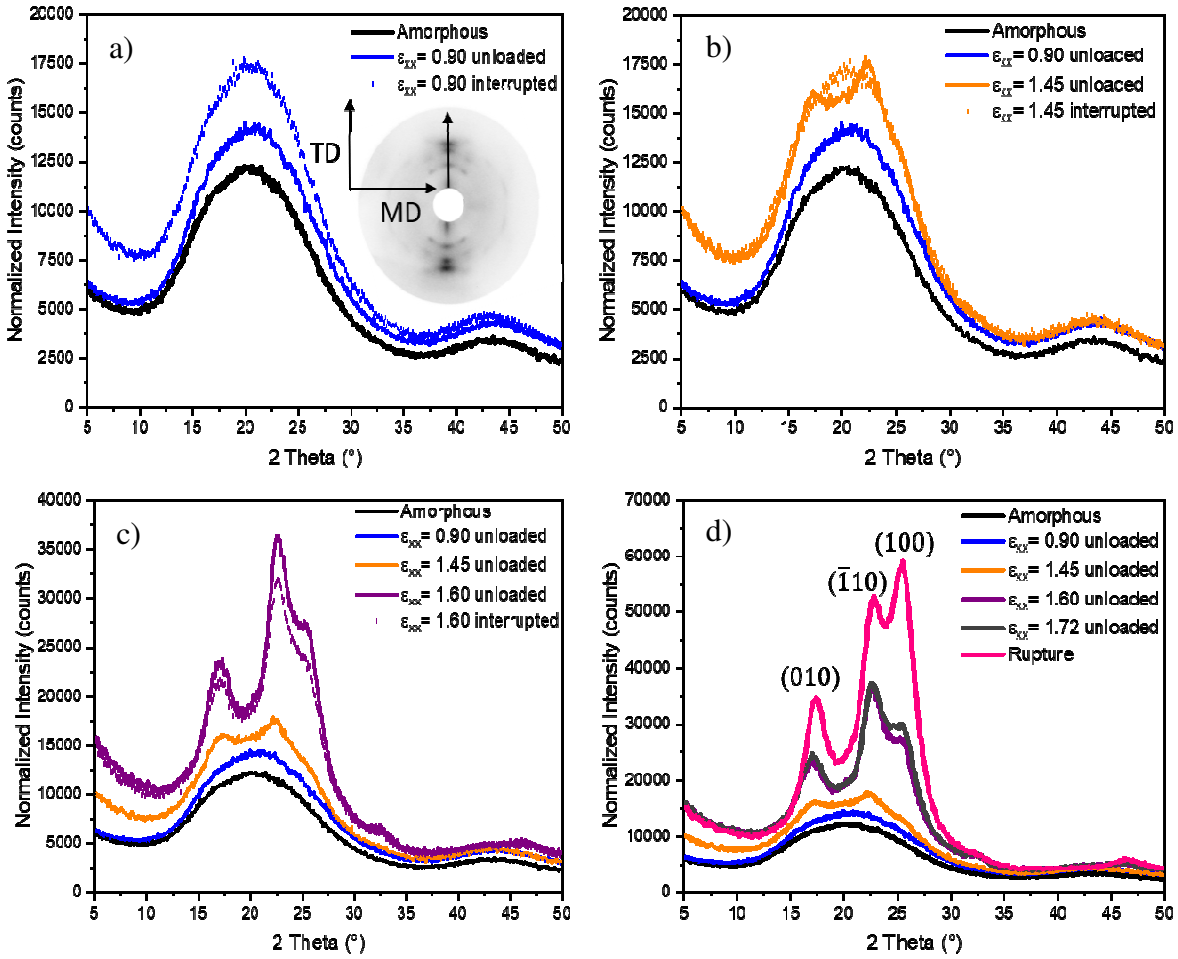


Figure 8. Diffraction scans in the transverse direction (TD): development of the PET crystalline phase for "interrupted" (dotted lines) and "unloaded" (plain lines) tests; (a) up to a strain of 0.90; (b) up to a strain of 1.45; (c) up to a strain of 1.60; (d) up to the rupture.

Figure 8 confirms qualitative observations deduced from Figure 5. PET remains amorphous, despite an increase in diffracted intensity, up to a strain of 1.45 (Figures 8.a and 8.b). In the earlier steps ($\varepsilon_{xx}$ = 0.90), the unloading path in temperature results in a decrease in intensity (compared to the interrupted test).

It is worth noticing that the early stage of stretching leading to an amorphous-like X-ray diffraction could be slightly crystalline according to DSC measurements (8 % if interrupted and 11 % if unloaded). One could argue that this contradiction results from experimental artefact and could be overestimated due to experimental uncertainness and to the dependence of enthalpy upon temperature (Eq. (2)). However, from a strain of 1.45, unloading makes it possible to distinguish two diffractions related to planes ($\bar{1}10$) and (010), whereas (100) one is still very weak but distinguishable as a shoulder. Conversely, interrupted sample could still

be considered as amorphous according to X-ray diffraction. DSC measurements, for their parts, leads to crystallinity ratios of 12 %, if interrupted, to 29 % when unloaded.

Furthermore, cold crystallization is a little fasten in the four cases compared to initial amorphous material (Figure 7) and the continuous and coherent evolution in crystallinity ratio encourages drawing some conclusions, even if reliability of DSC measurements is questionable in terms of precision. Indeed, this suggests that a certain level of organization could exist (chain orientation or something else) that is not immediately visible through X-ray diffraction and that could be small nuclei the number or the size of which increases upon unloading.

In any case, as described in the literature [4,31], the very first trace for periodic organisation can be related to hydrogen bonding interactions. The intensification can be the result of the organization of extended chains in denser zones that can be tighter and more periodic taking advantage of formation of those hydrogen bonds. The development of (100) plane peak which occurs later on could be related to $C_6$ ring mobility and flips in the tensile plane. This agrees with the literature, i.e. benzenic rings tends to be more and more organized and packed, in (100) plane of the crystal structure.

For low strain, amorphous phase appears less oriented in the case of "unloaded" tests, as this path can authorize chains relaxation in temperature. Moreover, if denser zones are too small to be stable they disappear upon unloading. Whereas at strain of 1.45 (Figure 8.b), the chain relaxation allows the stabilization of these zones. For this condition, PET has begun to form an organized microstructure, which is not yet a well-defined crystal. It is a metastable phase called mesophase which could be the crystal precursor or which could disappear.

For $\varepsilon_{xx} = 1.60$ (Figure 8.c), there are much less differences between the "interrupted" and the "unloaded" tests, even if the diffracted intensity increases with the unloading. Crystalline ratios still increase before (36 %) and after (42 %) unloading. The improvement of the third intense crystalline peak definition (100) does appear between $\varepsilon_{xx} = 1.45$ and $\varepsilon_{xx} = 1.60$, which is later than the two planes ($\bar{1}10$) and (010). The last unloaded condition before rupture, ($\varepsilon_{xx} = 1.72$, Figure 8.d), results in a structure closer to a "perfect" crystal compared to $\varepsilon_{xx} = 1.60$ but crystallinity ratio does not increase much (43 % *vs* 42 %). The mesophase is still better defined with the stretching and the unloading.

However, there is a significant change with the sample stretched up to the rupture (Figure 8.d). The diffracted intensities undergo an important increase, and the crystallinity ratio raises to 47%. This illustrates the efficiency in combining stress relaxation and low cooling rate to

develop crystallinity after stretching (cf. above discussion concerning Debye Scherrer patterns).

Finally, amorphous halo consists of two bumps, the second of which at an angle of 43°.corresponding to the $(\bar{1}05)$ refraction. The following meridional scans give some more information.

On Debye-Scherrer patterns, the signature associated to $(\bar{1}05)$ refraction is not visible. In the machine direction (MD), this crystalline family may become detectable thanks to quantitative scans. These measurements are presented in Figure 9.

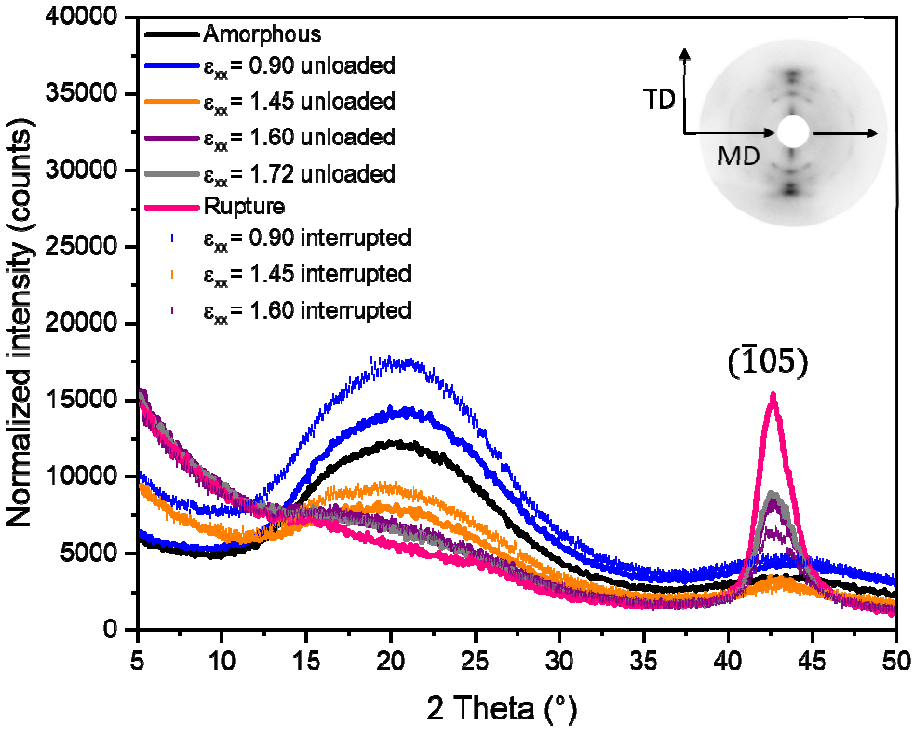


Figure 9. Diffraction scans in the machine direction (MD) for PET. Dots and lines are respectively relative to “interrupted” and “unloaded” samples.

In the meridional direction (machine direction), the amorphous halo intensity increases as a function of the stretching until a deformation of 0.90 and then decreases. Up to a deformation of 0.90, amorphous halo intensities are equivalent whatever the scanning direction is, both for “interrupted” and “unloaded” tests. No clear microstructural anisotropy is detectable. Nevertheless, some local amorphous phase organization may take place in both directions with an equilibrated manner. For higher deformations, above 1.45, microstructural anisotropy develops as described on Debye-Scherrer pattern. The amorphous halo periodicities are

getting more and more observable in the equatorial direction and become less and less visible in the meridional direction.

Step by step, the mesophase is getting more and more obvious, followed by the crystal appearance.

The bump around 43° observable in the initial amorphous PET as well as for low strain stretched samples becomes thinner from strain of 1.45. This peak is more intense for the "unloaded" test (orange line), compared to the "interrupted" one (orange dots). After the unloading, lateral organisation is visible on Figure 8.b, but organization perpendicularly to the stretching direction is not yet evidenced. At higher strain, when $\varepsilon_{xx} = 1.60$, the peak is formed and is, once again, more intense after the unloading. Chains organization is then optimum, promoting, along and perpendicularly to the chain axis, longitudinal and lateral periodicities which allows optimising interactions in all planes (H and $\phi-\phi$ bonds). Chains packing is then improved, and this organization becomes more and more probable as the stretching goes on.

### 3.2.2 PEF

The microstructural development observed in Figure 6 for PEF stretching is illustrated in Figure 10 thanks to the diffraction scans in the transverse direction (TD), observation of the (hk0) families. Crystalline families have already been indexed in previous papers [2,3,24].

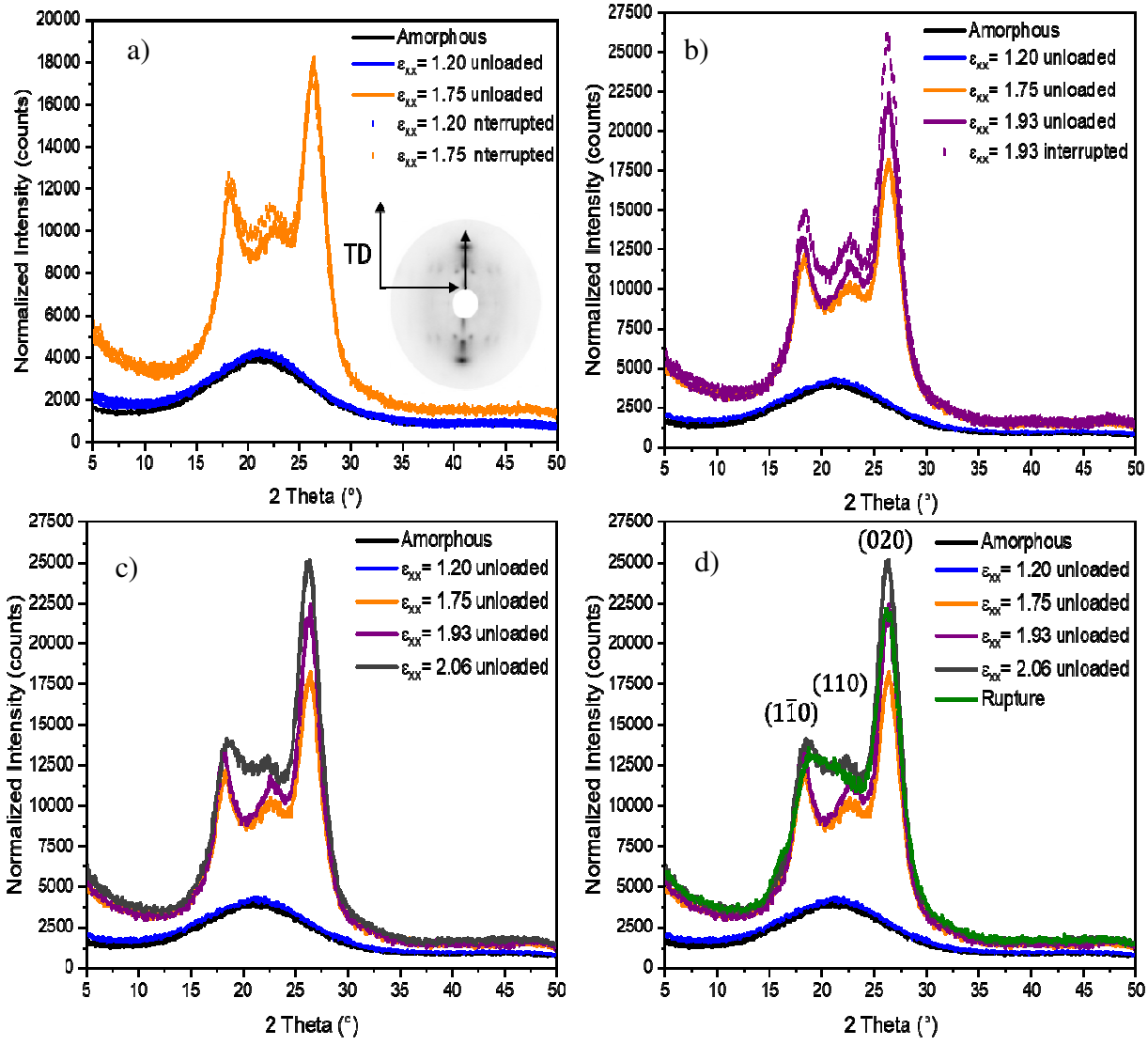


Figure 10. Diffraction scans obtained in the transverse direction (TD) : development of the PEF crystalline phase for “interrupted” and “unloaded” tests; (a) up to a strain of 1.75; (b) up to a strain of 1.93; (c) up to a strain of 2.06; (d) up to the rupture. Dots and lines are respectively relative to “interrupted” and “unloaded” samples.

The first “interrupted” and “unloaded” stretching condition (Figure 10.a, $\varepsilon_{xx} = 1.20$) exhibits a close to fully amorphous microstructure as it was observed in Figure 6 for both “interrupted” and “unloaded” samples. Associated crystallinity ratios are close to 0%. The amorphous halo of the “interrupted” test is slightly more intense, compared to the “unloaded” sample. For the unloaded sample, possible disorientation of the amorphous phase, due to chains relaxation, may have occurred. When the deformation is stopped just before the NDR ($\varepsilon_{xx} = 1.75$, Figure 10.a), the crystal is wholly formed, even before the unloading. The reported crystalline ratios are 27 % and 32%, for respectively interrupted and unloaded tests. Contrary to PET three

intense diffraction peaks can be observed. Moreover, the peaks intensity decreases slightly with the unloading. This can be explained by a disorientation of the crystal towards others directions or by a disappearance of PEF crystal during the unloading. As the crystalline amount increases a bit, the first hypothesis could be more relevant. These hypotheses will be developed further in the paper. Indeed, it was shown in previous works that PEF crystal is defined in equatorial, meridional but also in other directions [2,3,24].

The same scenario is found just after the NDR of ($\varepsilon_{xx}$ = 1.93; Figure 10.b). The "interrupted" samples is associated to more intense peaks, compared to the "unloaded" one. Crystalline ratio is lower for the interrupted test (28 %) than for the unloaded one (35 %). For a strain of 1.93, both samples exhibit peaks intensity higher than the sample unloaded before the strain hardening occurrence (orange curve, $\varepsilon_{xx}$ = 1.75).

For the last "unloaded" condition ($\varepsilon_{xx}$ = 2.06, Figure 10.c), the crystalline intensity increases again. Crystalline ratio is close to the previous unloaded condition (34 %). Nevertheless, the definition of the peaks changes. Up to now, three well-defined peaks were observable but from this point, the first and the second peaks become closer and wider. This trend continues to exist when the sample is stretched until its rupture. Indeed, the peak intensity of the (020) family decreases slightly. The merging of the first and the second peak is clearly visible, as a bump is formed, while the two crystalline families remain distinguishable. It seems that when PEF is stretched to high level of deformation, its first crystal formed (before the NDR) can be deformed and maybe slightly unstructured, if the stretching goes on. Final crystalline ratio is of 35%.

When the sample to screen distance decreases down to 30 mm, additional diffuse diffractions become observable (Figure 11), close to the meridional direction.

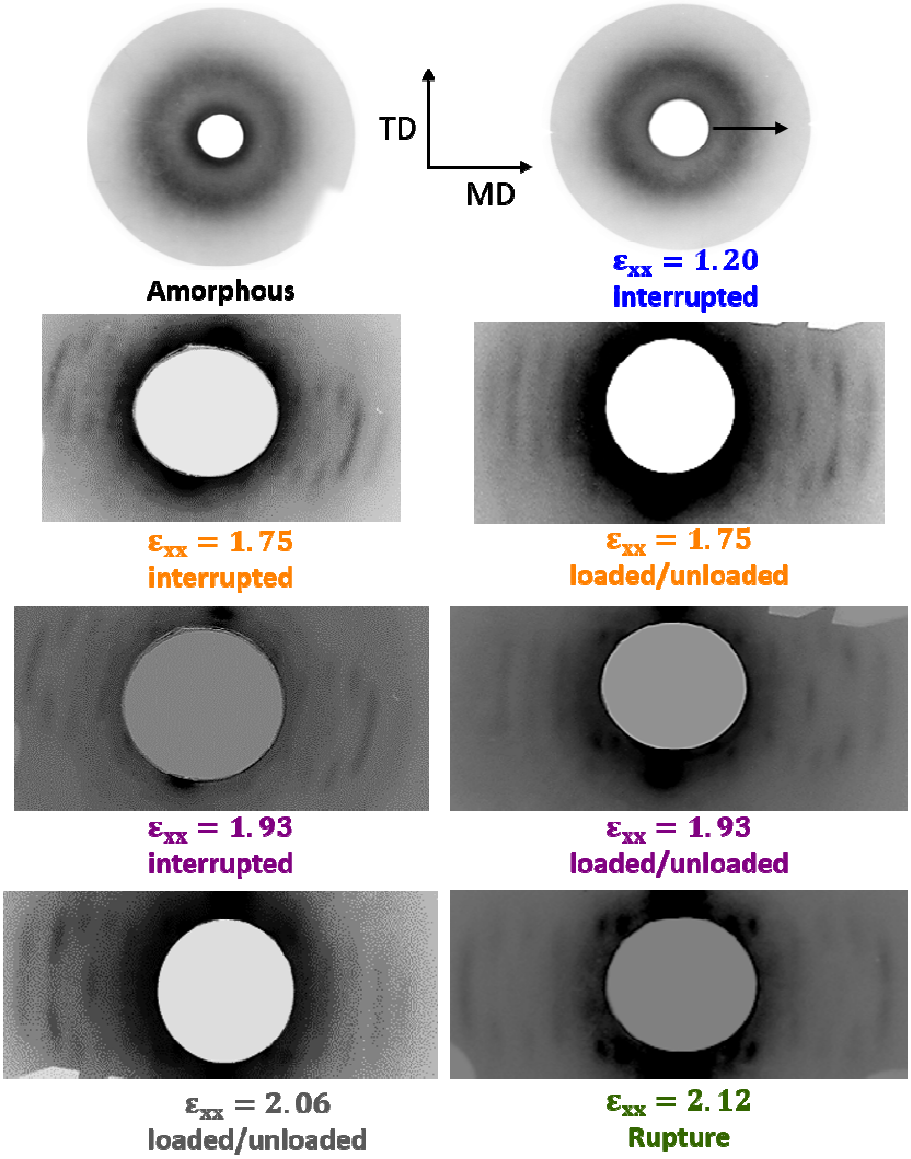


Figure 11. Debye Scherrer analysis of ”interrupted” and ”unloaded” PEF samples, with a sample-screen distance of 30 mm.

In Figure 11, two situations are depicted. When deformation has been performed up to $\varepsilon_{xx}$ = 1.20, the amorphous halo is observable similarly to the initial amorphous sample, which is the signature of an isotropic structure. This is observed for both “interrupted” and “unloaded” samples, even if only the result of “interrupted” sample is presented here. When the stretching develops, the same structure was found (as in Figure 6). These crystal families appear at the same time as those observed in Figure 6. It is difficult to discuss the intensity of the spots as they correspond more to diffuse arcs than spots. Nevertheless, it can be concluded that a crystalline phase appears as a whole in PEF, and that no intermediate organizations are stable enough to be observed. It is different from PET, where stretching seems to first lead to an

inner second step organization promoting along chain periodicity. This allows observation of the ($\bar{1}05$) peak in a postponed manner. It can be suggested that the main responsible of these differences is the furan ring that cannot flip into tensile plane and does not promote same level of interactions between constitutive units.

## 3.3 Properties induced by the stretching

Figures 12 and 13 show DMTA measurements carried out for the various samples stretched in conditions presented in Table 1. DMTA analysis is expected to address residual mobility of amorphous phase even if in a quite indirect manner.

### 3.3.2 PET amorphous phase mobility and rigidity evolution

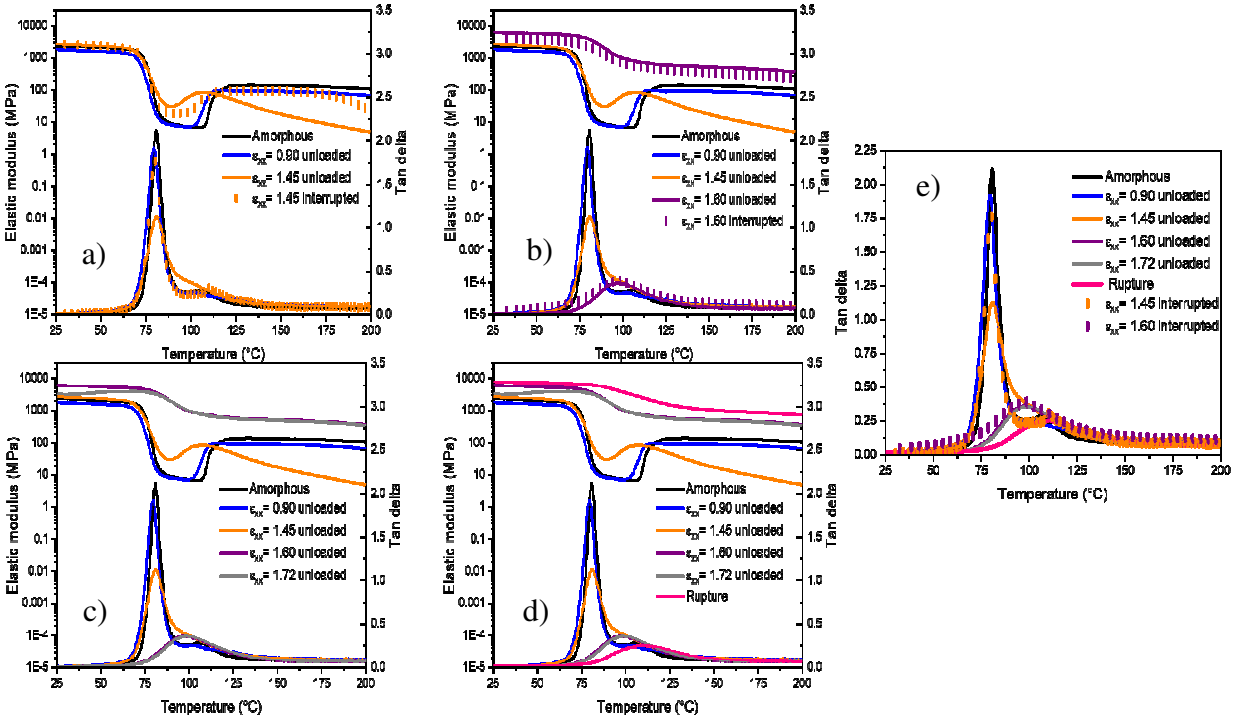


Figure 12. PET DMTA analysis performed at 1°C/min for "interrupted" and "unloaded" tests; (a) up to a strain of 1.45; (b) up to a strain of 1.60; (c) up to a strain of 1.72; (d) up to the rupture; (e) zoom on Tan delta evolution. Dots and lines are respectively relative to "interrupted" and "unloaded" samples.

For low strain condition ($\varepsilon_{xx}$ = 0.90), the elastic modulus at the glassy plateau is slightly lower than in the case of the initial amorphous sample (Figure 12.a). It is likely that processing of films induced some orientation in the material that was relaxed during heating stage of our

tensile protocol. Stretching up to strain of 0.90 could not be enough to re-orient material to the same extend.

In an equivalent manner to DSC, during DMTA tests for this sample stretched up to a low strain, cold crystallisation occurs at lower temperature. Nevertheless, modulus at rubbery plateau does not vary, suggesting that apparent entanglement density has not significantly evolved over stretching (or decreased while reaching glass transition). The microstructural change remains weak.

When a strain of 1.45 is reached (orange dots curve and orange line), elastic modulus at glassy plateau slightly increases; crystallization temperature is decreased in such a way that rubbery plateau disappears. In the case of "interrupted" samples, this effect is less important. It confirms DSC observations, with a real difference in cold crystallization between interrupted and unloaded PET. The $\alpha$–relaxation temperature does not increase significantly and ranges from 79 °C to 81 °C when strain ranges from 0 to 1.45.

For higher strains, no evidence for cold crystallisation is observed anymore and $\alpha$–relaxation temperature increases from 98 °C to 110 °C (Figures 12.c to 12.d). Both the glassy and rubbery plateau increase.

### 3.3.3 PEF amorphous phase mobility and rigidity evolution

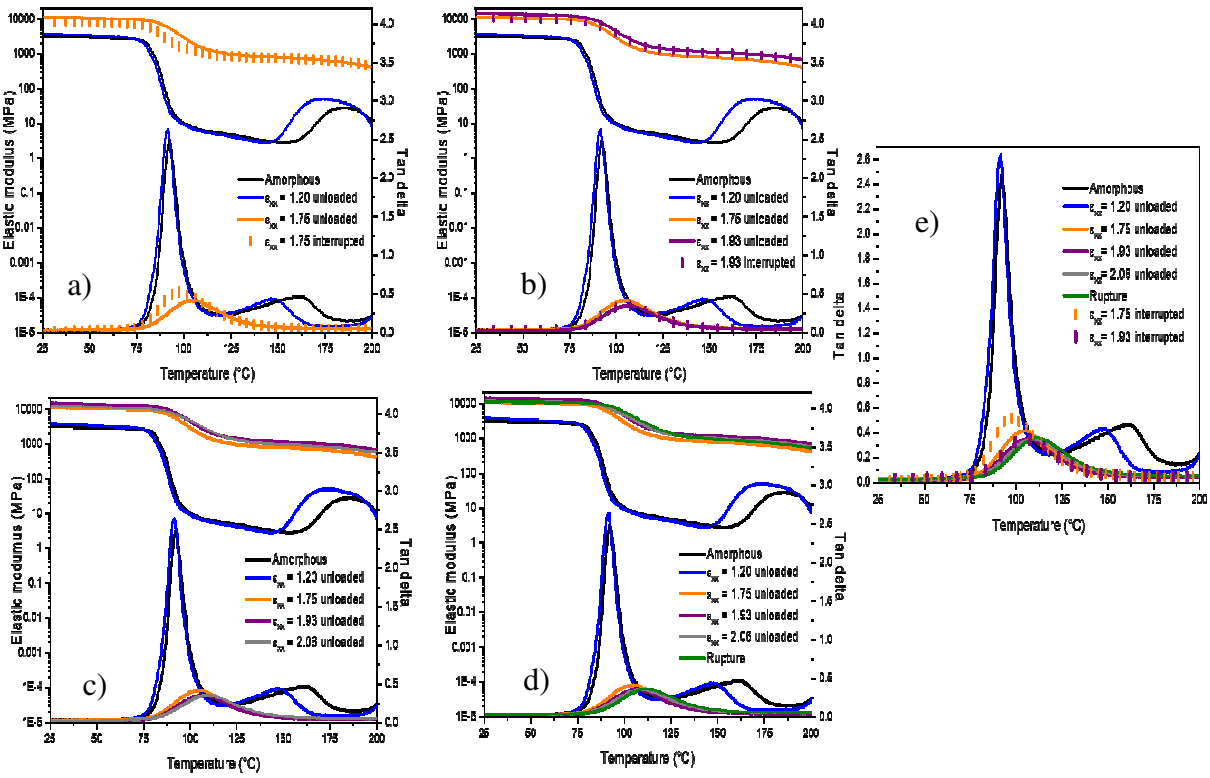


Figure 13. PEF DMTA analysis performed at 1°C/min for "interrupted" and "unloaded" tests; (a) up to a strain of 1.75; (b) up to a strain of 1.93; (c) up to a strain of 2.06; (d) up to the rupture; (e) zoom on Tan delta evolution. Dots and lines are respectively relative to "interrupted" and "unloaded" samples.

The same qualitative observations can be done for PEF (Figure 13). Low strain ($\varepsilon_{xx}$ = 1.20) results in a decrease of cold crystallisation temperature, which was not visible on DSC scans, as the heating rate was ten times higher (1 °C/min *vs* 10 °C/min). High strains lead to an increase in $T_\alpha$ (up to 112 °C) and to an increase of moduli. The increase of the $\alpha$–relaxation temperature along the stretching, as well as the decrease of the chain mobility, is clearly visible in Figure 13.e. where the amorphous phase is getting more and more constrained by the crystalline phase. This evolution is not really progressive and is sharper than for PET. Some microstructural changes, as the crystal improvement, until the sample rupture, may still exist in PEF even if the crystal is formed before the strain hardening.

To conclude, the formation of PEF crystal occurs before NDR. DMTA results are in good agreement with previous results and give additional information on remaining potential crystallisation and on $\alpha$–relaxation. The relatively slow heating rate in DMTA suits better with the PEF crystallization rate, as it allows to observe crystallization compared to DSC.

### 3.3.3. Conformational evolution during PET and PEF crystal development

During the crystalline phase formation, conformational changes of the ethylene glycol group from *gauche* conformation to *trans* conformation occur. This phenomenon corresponds to the chain extension. IR spectroscopy reveals these conformational evolutions by the appearance of 1470 $cm^{-1}$ and 1480 $cm^{-1}$ peaks for PET and PEF, respectively. In addition, the peak intensity at 1340 $cm^{-1}$ increases for both materials when crystallization occurs [25].

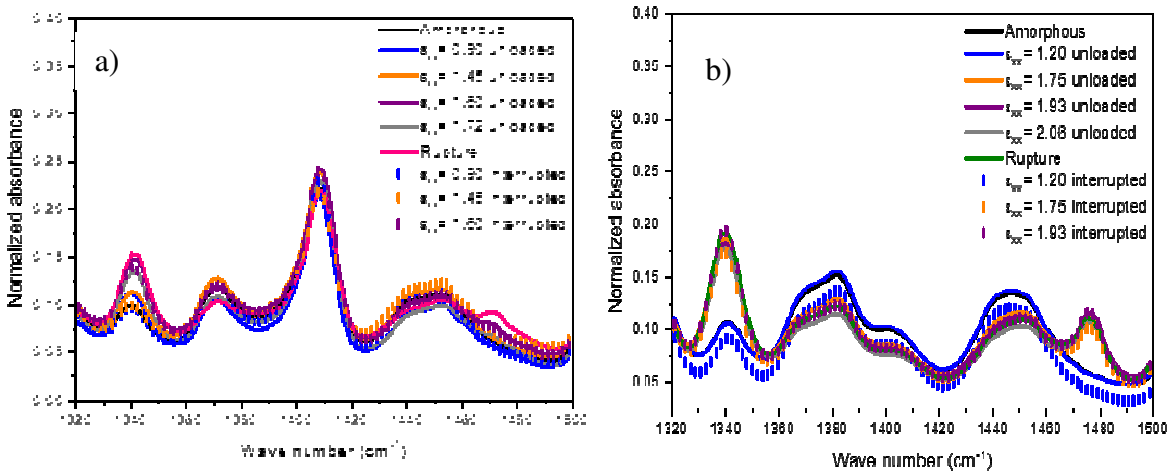


Figure 14. FT–IR spectra from 1320 to 1500 $cm^{-1}$ of (a) PET and (b) PEF for "unloaded" and "interrupted" samples. Dots and lines are respectively relative to "interrupted" and "unloaded" samples.

Concerning PET, it is possible to distinguish three cases (Figure 14.a): for both "interrupted" and "unloaded samples", when $\varepsilon_{xx} = 1.60$, $\varepsilon_{xx} = 1.72$ and when the sample has been stretched up to its rupture, there is a real increase of the peak at 1340 $cm^{-1}$. With the stretching, the number of ethylene glycol present in *trans* conformation increases: the creation of a crystal or of a more "constrained" amorphous phase takes place. The two others "interrupted" conditions ($\varepsilon_{xx} = 0.90$, blue dots, and $\varepsilon_{xx} = 1.45$, orange dots) are well superimposed with the amorphous sample. It means that, there is a minority of ethylene glycol in *trans* conformation in all these samples, and a majority of *gauche* conformations. For the two others "unloaded" conditions ($\varepsilon_{xx} = 0.90$, blue line, and $\varepsilon_{xx} = 1.45$, orange line), there is also an increase of *trans* conformations, leading to an intermediary state between the amorphous sample with a majority of *gauche* conformations and the crystal formation itself with its majority of *trans* conformation. This is relevant with our previous observations. For the peak at 1470 $cm^{-1}$, the same conclusions can be drawn.

Concerning PEF, the situation is more binary as shown in Figure 14.b. The spectra corresponding to the amorphous sample, the "unloaded" and the "interrupted" for $\varepsilon_{xx} = 1.20$ are well superimposed. It is in adequation with the previous result and with the amorphous

structure of these samples (with a majority of *gauche* conformation). For all the other conditions, the presence of *trans* conformations becomes obvious with the increase of the peaks at 1340 $cm^{-1}$ and 1480 $cm^{-1}$. All the curves are superimposed. It confirms that the crystal of PEF is well-formed before the beginning of the strain hardening, and remains almost the same after unloading or rupture.

## 4. Conclusions

The microstructural evolution over uniaxial stretching of PEF and PET was investigated. It was observed that SIC occurs in PEF and in PET when relevant strain-rate/temperature conditions are applied. Natural draw ratio is lower for PET than for PEF. This could be related to the easier change in local conformations of the benzenic ring compared to furan one. Combined effects of this higher mobility and of the strength of interaction between constitutive units makes it possible to promote mesophase or imperfect crystal in PET that contribute to hardening. Consequently, well-defined crystal may exist or not in stretched PET, depending on cooling protocols after stretching and on the amount of stretching. For PEF, well-defined crystal is the only way to promote strain hardening. Mechanical tests show that the strain hardening slope is sharper for PEF compared to PET which continues to improve its mesophase during it. PEF crystal remains almost the same from its first appearance until the end of the stretching even if some crystal improvements may occur. In parallel, the $\alpha$–relaxation temperature increases with stretching (up to 113°C) depending on both stretching and unloading conditions. This dependency is clearly observable before the NDR but remains far less obvious over the strain hardening where the crystal no longer changes.

## 5. Acknowledgements

This work was supported by the French Environment and Energy Management Agency (ADEME) and Sidel as well as Avantium Renewable Polymers

## References

[1] G. Stoclet, J.M. Lefebvre, B. Yeniad, G. Gobius du Sart, S. de Vos, On the strain-induced structural evolution of Poly(ethylene-2,5-furanoate) upon uniaxial stretching: An in-situ SAXS-WAXS study, Polymer (Guildf). 134 (2018) 227–241. doi:10.1016/j.polymer.2017.11.071.

[2] Y. Mao, D.G. Bucknall, R.M. Kriegel, Synchrotron X-ray scattering study on amorphous poly(ethylene furanoate) under uniaxial deformation, Polymer (Guildf). 139 (2018) 60–67. doi:10.1016/j.polymer.2018.01.062.

[3] Y. Mao, R.M. Kriegel, D.G. Bucknall, The crystal structure of poly(ethylene furanoate), Polymer (Guildf). 102 (2016) 308–314. doi:10.1016/j.polymer.2016.08.052.

[4] E. Gorlier, J.M. Haudin, N. Billon, Strain-induced crystallisation in bulk amorphous PET under uni-axial loading, Polymer (Guildf). 42 (2001) 9541–9549. doi:10.1016/S0032-3861(01)00497-9.

[5] D. Kawakami, C. Burger, S. Ran, C. Avila-Orta, I. Sics, B. Chu, S.M. Chiao, B.S. Hsiao, T. Kikutani, New insights into lamellar structure development and SAXSA/WAXD sequence appearance during uniaxial stretching of amorphous polyethylene terephthalate above glass transition temperature, Macromolecules. 41 (2008) 2859–2867. doi:10.1021/ma702554t.

[6] D.R. Salem, Development of crystalline order during hot-drawing of poly(ethylene terephthalate) film: influence of strain rate, Polymer (Guildf). 33 (1992) 3182–3188. doi:10.1016/0032-3861(92)90232-L.

[7] G. Le Bourvellec, J. Beautemps, Stretching of PET films under constant load. II. Structural analysis, J. Appl. Polym. Sci. 39 (1990) 329–339. doi:10.1002/app.1990.070390210.

[8] G.E. Welsh, D.J. Blundell, A.H. Windle, A transient mesophase on drawing polymers based on polyethylene terephthalate (PET) and polyethylene naphthoate (PEN), J. Mater. Sci. 35 (2000) 5225–5240. doi:10.1023/A:1004820824004.

[9] A. Ajji, J. Guèvremont, K.C. Cole, M.M. Dumoulin, Orientation and structure of drawn poly(ethylene terephthalate), Polymer (Guildf). 37 (1996) 3707–3714. doi:10.1016/0032-3861(96)00175-9.

[10] D.J. Blundell, A. Mahendrasingam, C. Martin, W. Fuller, D.H. MacKerron, J.L. Harvie, R.J. Oldman, C. Riekel, Orientation prior to crystallisation during drawing of poly(ethylene terephthalate), Polymer (Guildf). 41 (2000) 7793–7802. doi:10.1016/S0032-3861(00)00128-2.

[11] D.J. Blundell, D.H. MacKerron, W. Fuller, A. Mahendrasingam, C. Martin, R.J. Oldman, R.J. Rule, C. Riekel, Characterization of strain-induced crystallization of poly(ethylene terephthalate) at fast draw rates using synchrotron radiation, Polymer (Guildf). 37 (1996) 3303–3311. doi:10.1016/0032-3861(96)88476-X.

[12] A. Mahendrasingam, C. Martin, W. Fuller, D.J. Blundell, R.J. Oldman, D.H. MacKerron, J.L. Harvie, C. Riekel, Observation of a transient structure prior to strain-induced crystallization in poly(ethylene terephthalate), 2000. doi:10.1016/S0032-3861(99)00461-9.

[13] S. Ran, Z. Wang, C. Burger, B. Chu, B.S. Hsiao, Mesophase as the precursor for strain-induced crystallization in amorphous poly(ethylene terephthalate) film, Macromolecules. 35 (2002) 10102–10107. doi:10.1021/ma021252i.

[14] Y. Marco, L. Chevalier, G. Régnier, A. Poitou, Induced crystallization and orientation of poly(ethylene terephthalate) during uniaxial and biaxial elongation, Macromol. Symp. 185 (2002) 15–34. doi:10.1002/1521-3900(200208)185:1<15::AID-MASY15>3.0.CO;2-J.

[15] S.K. Burgess, J.E. Leisen, B.E. Kraftschik, C.R. Mubarak, R.M. Kriegel, W.J. Koros, Chain Mobility, Thermal, and Mechanical Properties of Poly(ethylene furanoate) Compared to Poly(ethylene terephthalate), Macromolecules. 47 (2014) 1383–1391. doi:10.1021/ma5000199.

[16] A. Codou, M. Moncel, J.G. van Berkel, N. Guigo, N. Sbirrazzuoli, Glass transition dynamics and cooperativity length of poly(ethylene 2,5-furandicarboxylate) compared to poly(ethylene terephthalate), Phys. Chem. Chem. Phys. 18 (2016) 16647–16658. doi:10.1039/C6CP01227B.

[17] R.J.I. Knoop, W. Vogelzang, J. van Haveren, D.S. van Es, High molecular weight poly(ethylene-2,5-furanoate); critical aspects in synthesis and mechanical property determination, J. Polym. Sci. Part A Polym. Chem. 51 (2013) 4191–4199. doi:10.1002/pola.26833.

[18] T. Dimitriadis, D.N. Bikiaris, G.Z. Papageorgiou, G. Floudas, Molecular Dynamics of Poly(ethylene-2,5-furanoate) (PEF) as a Function of the Degree of Crystallinity by Dielectric Spectroscopy and Calorimetry, Macromol. Chem. Phys. 217 (2016) 2056–2062. doi:10.1002/macp.201600278.

[19] A. Codou, N. Guigo, J. Van Berkel, E. De Jong, N. Sbirrazzuoli, Non-isothermal Crystallization Kinetics of Synthesized via the Direct Esterifi cation Process, (n.d.) 2065–2074.

[20] S.K. Burgess, O. Karvan, J.R. Johnson, R.M. Kriegel, W.J. Koros, Oxygen sorption and transport in amorphous poly(ethylene furanoate), Polymer (Guildf). 55 (2014) 4748–4756. doi:10.1016/j.polymer.2014.07.041.

[21] S.K. Burgess, D.S. Mikkilineni, D.B. Yu, D.J. Kim, C.R. Mubarak, R.M. Kriegel, W.J. Koros, Water sorption in poly(ethylene furanoate) compared to poly(ethylene terephthalate). Part 2: Kinetic sorption, Polymer (Guildf). 55 (2014) 6870–6882. doi:10.1016/J.POLYMER.2014.10.065.

[22] R.D.. B. Daubeny, The crystal structure of polyethylene terephthalate, Proc. R. Soc. London. Ser. A. Math. Phys. Sci. 226 (1954) 531–542. doi:10.1098/rspa.1954.0273.

[23] L.G. Kazaryan, F.M. Medvedeva, X-Ray study of the structure of the polyester of furan-2, 5-dicarboxylic acid, Vysok. Soedin., Ser. B. 10 (1968).

[24] E. Forestier, C. Combeaud, N. Guigo, G. Monge, J.M. Haudin, N. Sbirrazzuoli, N. Billon, Strain-induced crystallization of poly(ethylene 2,5-furandicarboxylate). Mechanical and crystallographic analysis, Polymer (Guildf). (2020). doi:10.1016/j.polymer.2019.122126.

[25] C.F. Araujo, M.M. Nolasco, P.J.A. Ribeiro-Claro, S. Rudić, A.J.D. Silvestre, P.D. Vaz, A.F. Sousa, Inside PEF: Chain Conformation and Dynamics in Crystalline and Amorphous Domains, Macromolecules. 51 (2018) 3515–3526. doi:10.1021/acs.macromol.8b00192.

[26] E. Forestier, N. Guigo, C. Combeaud, N. Billon, N. Sbirrazzuoli, Conformational changes analysis of PEF (polyethylene 2,5-furandicarboxylate), and PET (polyethylene terephthalate) under uniaxial stretching, Macromolecules, submitted. (2020).

[27] G. Stoclet, G. Gobius du Sart, B. Yeniad, S. de Vos, J.M. Lefebvre, Isothermal crystallization and structural characterization of poly(ethylene-2,5-furanoate), Polymer (Guildf). 72 (2015) 165–176. doi:10.1016/j.polymer.2015.07.014.

[28] J.G. van Berkel, N. Guigo, H.A. Visser, N. Sbirrazzuoli, Chain Structure and Molecular Weight Dependent Mechanics of Poly(ethylene 2,5-furandicarboxylate)

Compared to Poly(ethylene terephthalate), Macromolecules. 51 (2018) 8539–8549. doi:10.1021/acs.macromol.8b01831.

[29] C. Menager, N. Guigo, L. Martino, N. Sbirrazzuoli, H. Visser, S.A.E. Boyer, N. Billon, G. Monge, C. Combeaud, Strain induced crystallization in biobased Poly(ethylene 2,5-furandicarboxylate) (PEF); conditions for appearance and microstructure analysis, Polymer (Guildf). 158 (2018) 364–371. doi:10.1016/J.POLYMER.2018.10.054.

[30] G.Z. Papageorgiou, V. Tsanaktsis, D.N. Bikiaris, Synthesis of poly(ethylene furandicarboxylate) polyester using monomers derived from renewable resources: thermal behavior comparison with PET and PEN, Phys. Chem. Chem. Phys. 16 (2014) 7946–7958. doi:10.1039/C4CP00518J.

[31] M. Picard, Strain induced crystallisation during stretch blow moulding of PET; correlation with strain hardening, École Nationale Supérieure des Mines de Paris, 2008. https://pastel.archives-ouvertes.fr/tel-00343353.

[32] G. Quandalle, Study and mechanical modeling of the strain-induced-crystallization of polymers : crosslinked naturel rubber and PET, PSL Research University, 2017. https://pastel.archives-ouvertes.fr/tel-01774634.

[33] A. Mahendrasingam, C. Martin, W. Fuller, D.J. Blundell, R.J. Oldman, J.L. Harvie, D.H. MacKerron, C. Riekel, P. Engström, Effect of draw ratio and temperature on the strain-induced crystallization of poly (ethylene terephthalate) at fast draw rates, Polymer (Guildf). 40 (1999) 5553–5565. doi:10.1016/S0032-3861(98)00770-8.

[34] Y. Fu, W.R. Busing, Y. Jin, K.A. Affholter, B. Wunderlich, Structure analysis of the noncrystalline material in poly(ethylene terephthalate) fibers, Macromol. Chem. Phys. 195 (1994) 803–822. doi:10.1002/macp.1994.021950236.

[35] J. Liu, P.H. Geil, Crystal structure and morphology of poly(ethylene terephthalate) single crystals prepared by melt polymerization, J. Macromol. Sci. - Phys. 36 (1997) 61–85. doi:10.1080/00222349708220415.

[36] Handbook of Thermoplastic Polyesters, 2002. doi:10.1002/3527601961.

PET

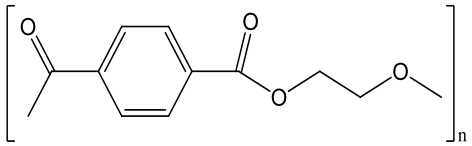

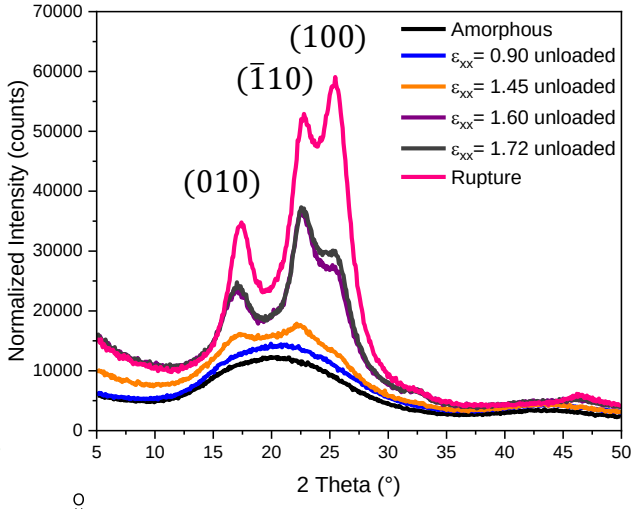


PEF

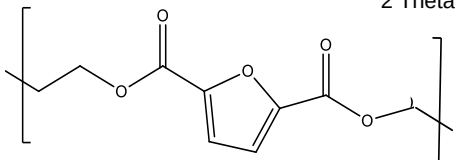

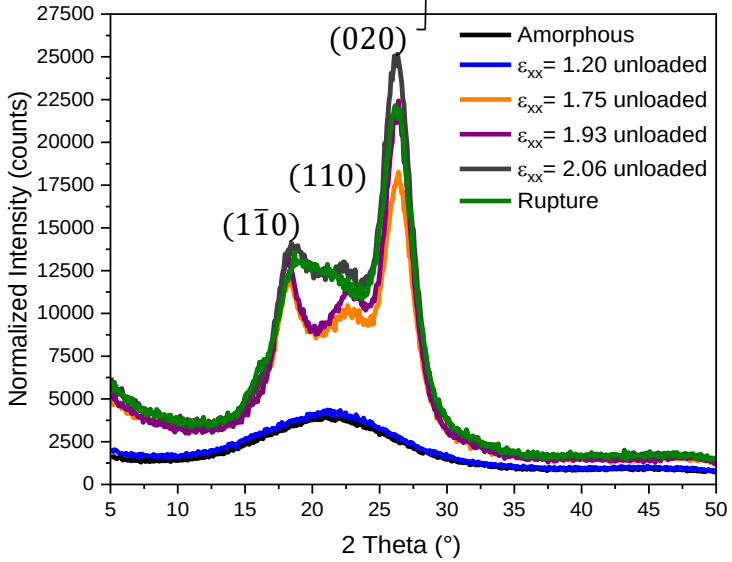


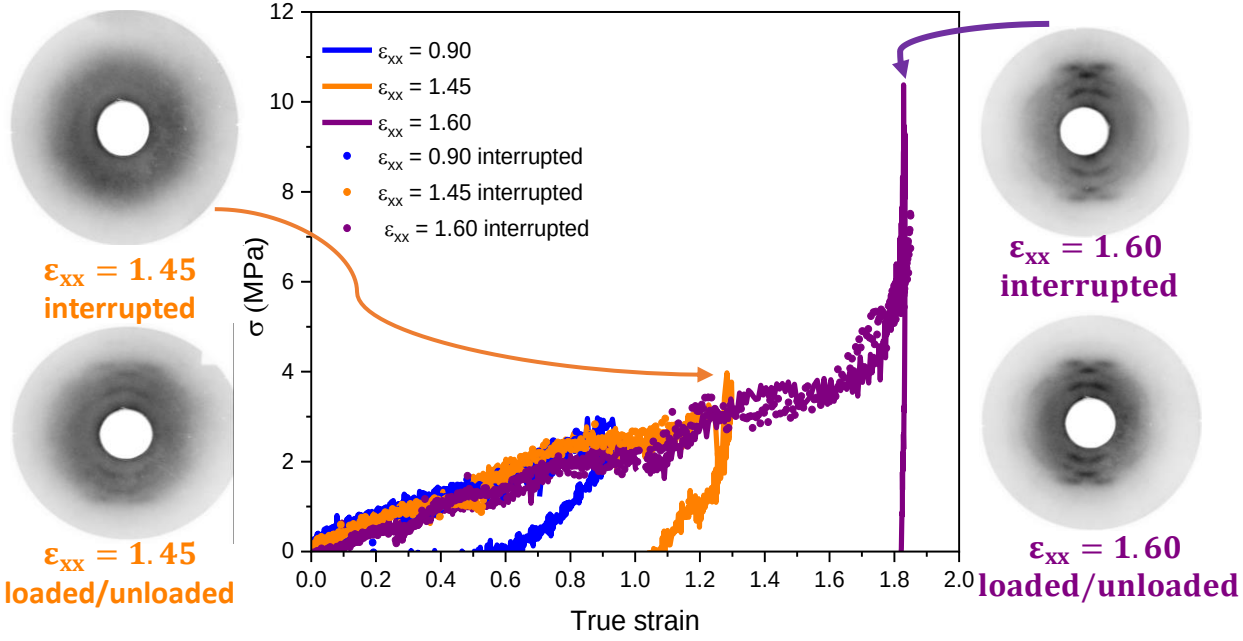


$\varepsilon_{xx} = 1.45$ interrupted

$\varepsilon_{xx} = 1.45$ loaded/unloaded

$\varepsilon_{xx} = 1.60$ interrupted

$\varepsilon_{xx} = 1.60$ loaded/unloaded

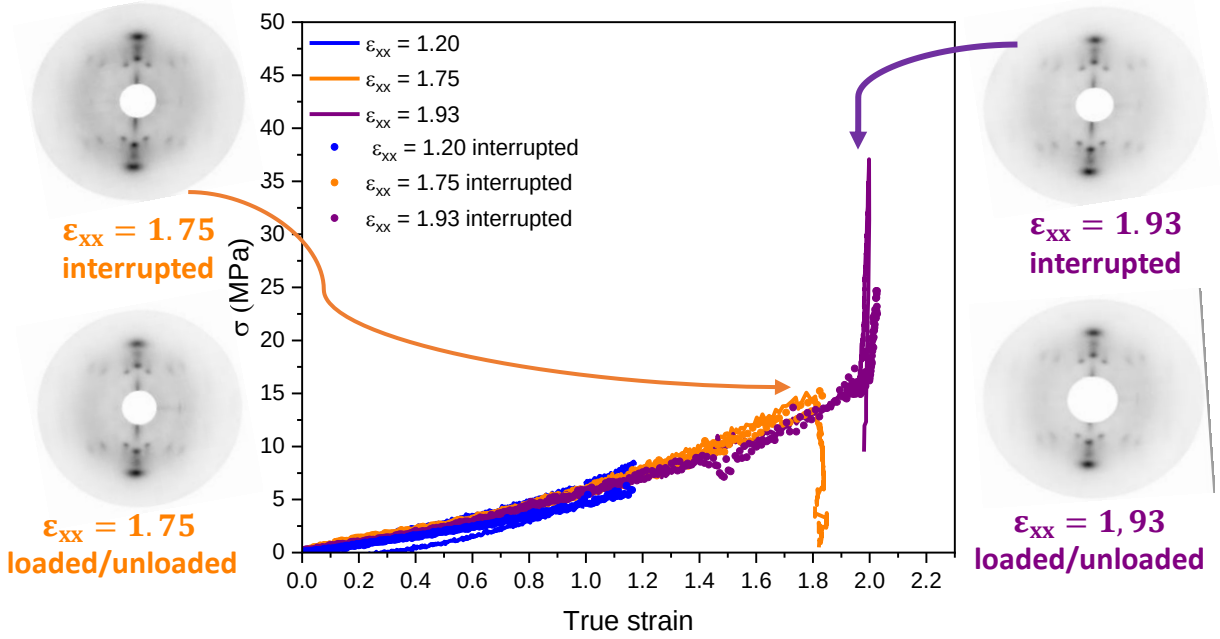


$\varepsilon_{xx} = 1.75$ interrupted

$\varepsilon_{xx} = 1.75$ loaded/unloaded

$\varepsilon_{xx} = 1.93$ interrupted

$\varepsilon_{xx} = 1,93$ loaded/unloaded